UDK 669.018.27:57.012.3
Original scientific article/Izvirni znanstveni članek

ISSN 1580-2949
Mater. Tehnol.

EXPLORING CORROSION RESISTANCE AND MICROSTRUCTURE OF MANGANESE PHOSPHATE CONVERSION COATING ON 65Mn SPRING STEEL

RAZISKAVA KOROZIJSKE ODPORNOSTI IN MIKROSTRUKTURE KONVERZIJSKE PREVLEKE NA OSNOVI MANGAN FOSFATA, NANEŠENE NA VZMETNO JEKLO VRSTE 65Mn

Peng-fei Zhang[1,2,3*], Ke-yao Li[2], Gang Ji[2], Qi Liu[2], Long-fei Xie[2] , Lin-Feng Wei[2], De-cheng Wang[3]

[1]University of Science and Technology Beijing, 30 Xueyuan Road, Haidian District, Beijing, 100083, P.R. China
[2]China Xi'an Rare Metal Materials Institute Co., Ltd., 96 Weiyang Road, Xi'an, 710016, P.R. China
[3]China Academy of Machinery Science and Technology, 2 Shouti Road, Haidian District, Beijing, 100044, P.R. China

Prejem rokopisa – received: 2024-05-20; sprejem za objavo – accepted for publication: 2024-09-25

doi:10.17222/mit.2024.1198

Manganese phosphate conversion coatings were prepared on 65Mn spring steel. The surface morphologies and compositions of the coatings were examined through scanning electron microscopy (SEM) and X-ray diffraction (XRD). The corrosion resistance of the coatings was investigated using a copper sulfate titration experiment, salt spray test and electrochemical corrosion test. The results showed that a uniform and dense coating was obtained when the acid ratio was 10, the phosphating temperature was 85 °C, and the phosphating time was 5 min. There was no obvious rust on the manganese phosphate coating surface after 48 h of salt spray. Ultimately, the growth mechanism and corrosion behavior of the manganese phosphate conversion coating are explained.

Keywords: 65Mn spring steel, manganese phosphate, microstructure, corrosion resistance

Avtorji so pripravili konverzijsko prevleko na osnovi mangan-fosfata na vzmetnem jeklu vrste 65Mn. Morfologijo površine in sestavo prevleke so analizirali s pomočjo vrstičnega elektronskega mikroskopa (SEM) in rentgenske difrakcije (XRD). Korozijsko odpornost prevleke so preiskovali s pomočjo titracije bakrovega sulfata, testa s sprejem slanice in elektro-kemijskih korozijskih preiskav. Rezultati analiz so pokazali, da so izdelali enovito (homogeno) in gosto prevleko pri kislinskem razmerju 10, temperaturi fosfatiranja 85 °C in času fosfatiranja 5 min. Po 48 urni obdelavi s sprejem slanice avtorji niso opazili nobenega znaka očitnega rjavenja prevleke. Avtorji v tem prispevku na koncu razložijo še mehanizem rasti in korozijsko obnašanje izdelane mangan-fosfatne konverzijske prevleke.

Ključne besede: vzmetno jeklo vrste 65Mn, mangan-fosfat, mikrostrukture, korozijska odpornost

1 INTRODUCTION

65Mn steel is one of the famous spring materials with high strength and good capability of plastic deformation.[1] It is widely used for automobile suspension springs, leaf springs,[2] mechanical springs and so on.[3–4] However, springs in the process of manufacture, storage and use are often eroded by a moist atmosphere, salt fog in the sea atmosphere, and industrial waste gas and so on,[5–7] which makes its use limited. Thus, it is essential to enhance the corrosion resistance of the 65Mn steel surface and extend the fatigue life of springs.

At present, to improve the corrosion resistance, spring surfaces use anodic plating, polymer coating,[8] oxidation treatment,[9] micro-arc oxidation,[10] and so on. The chemical method allows us to make something prominent due to its simple operation and stability. Chromium salt treatment is an effective method of anticorrosion in traditional approaches, but it significantly increases carcinogenicity and is environmentally not friendly due to chromium being virulent.[11,12] The choice of environmentally friendly non-chromium coatings has aroused wide attention. Phosphate coating is widely used in the automotive, marine, aerospace, and manufacturing industries because of its low cost and high corrosion resistance.[13]

Manganese phosphate conversion coating is used for springs due to its low cost, and rapid action combined with corrosion-resistance and self-lubricating properties. Shanmugam et al. improved the quality of manganese phosphate coating on mild steel using permanganate as an additive to increase iron dissolution.[14] Guo et al. enhanced the corrosion resistance of Mn-P coating on Q235 steel by adjusting the phosphorus-manganese ratio.[15] Nikdehghan et al. investigated the surface morphology and corrosion resistance of Zn-Mn phosphate coating on AISI 4130 steel under different heat treatments.[16] A thin and dense phosphate coating was obtained when $Mn^{2+} : PO_4^{3-} = 1 : 7$. There was no obvious corrosion after 30-h salt spray. In order to improve the corrosion resistance of phosphate conversion coating on an

*Corresponding author's e-mail:
zhangpf1007@163.com (Peng-fei Zhang)

electrogalvanized steel sheet, Ni^{2+} and Mn^{2+} ions were added to the phosphate solution by Su.[17] Zang et al. researched the tribological properties of manganese phosphate conversion coatings on the AISI 52100 steel surface.[18] The results showed that the friction coefficients of Mn-PH coatings were reduced by 15 %. However, the formation of manganese phosphate conversion and the anti-corrosion properties of the coating on 65 Mn spring steel have been seldom reported.

In this study, the surface phosphating process (acid ratio, phosphating temperature and phosphating time) of 65 Mn spring steel was studied using the orthogonal test method. The anti-corrosion of phosphating conversion coating is researched using a copper sulfate titration experiment, salt spray test and electrochemical corrosion test. The microstructures and compositions of coatings applied using different phosphating processes on a 65Mn spring steel substrate were researched, and the corrosion resistance was evaluated. Simultaneously, the growth mechanism and corrosion behavior of manganese phosphate on the surface of 65 Mn spring steel were determined. Finally, the phosphating-process parameter combination was optimized to improve the corrosion resistance of the spring surface.

2 EXPERIMENTAL PART

Commercial 65Mn steel (composition in *w*/%: 0.64 C, 0.22 Si, 0.99 Mn, 0.003 S, 0.022 P, 0.16 Cr, 0.02 Ni, 0.04 Cu, with the balance being Fe) was cut into (20 × 12 × 3) mm samples. The substrate was ground with #400 to #1500 SiC abrasive paper and rinsed with deionized water. The specimens were degreased with an alkaline solution (10 *w*/% KOH) for 6 min at room temperature (RT), thereafter, they were cleaned with deionized water. The BT-320 powder of titanium phosphate salt at a concentration of 3–5 g/L (Dongguan Dingrun Chemical Technology Co., LTD.) was used as pre-dip for 1 min. After cleaning with deionized water, the sample surface was treated by manganese phosphating. The phosphating solution was mainly composed of Mn^{2+}, NO^{3-}, PO_4^{3-}, H_3PO_4, and other additives. The acid ratio was defined as the ratio of free acidity to total acidity. Orthogonal experiments with three factors and four levels were conducted, considering the following process parameters: acid ratio (4, 6, 8, and 10), phosphating temperature (65, 75, 85, and 95) °C, phosphating time (3, 5, 7, and 9 min). Phosphating temperature was controlled by a water bath kettle. The $H_2Cr_2O_7$ (0.3–0.45 g/L, pH 2–4) solution was used for phosphating post-treatment passivation at 50 °C for 2 min.

After the phosphating experiments, the sample surfaces were analyzed using scanning electron microscopy (SEM, GeminiSEM 500). The phase constitution of the coatings were analyzed using X-ray diffraction (XRD, Rigaku D/max-2500/PC) with CuKα radiation. The corrosion resistance of phosphate coatings was determined using the $CuSO_4$ drop method in accordance with the GB6807-86 standard. When 1–2 drops of the solution are applied to the phosphate coating, a color change from blue to yellow or light red is observed. The solution is composed of 40 mL $CuSO_4$ (0.25 mol/L), 0.8 mL HCl (0.10 mol/L) and 20 mL NaCl (10 %).

The phosphating coatings were removed by a 50 g/L CrO_3 solution at 75 °C for 15 min in accordance with the GB/T 9792-2003 standard, and then cleaned with deionized water. Each sample used a new solution. The mass of the samples and removal of the coatings were denoted as m_1 and m_2, respectively. A was the phosphating-coating surface area. The weight of the phosphating coating was calculated with the following formula:

$$m_A = \frac{m_1 - m_2}{A} \times 10^4 \quad (1)$$

A salt-spray test was performed in a salt-spray test chamber (Beijing Donggong Lianhua Scientific Instrument and Equipment Co., LTD, YWX-1200) in accordance with the GB/T 10125-1997 standard. The 5 % NaCl solution was used as the corrosion medium spray, and the salt spray volume was 1–2 mL/min. The test chamber temperature was 35 °C for 48 h. The corrosion resistance of the coatings was tested using a standard three-electrode cell (CHI660E) in a 3.5 *w*/% NaCl aqueous solution. The auxiliary electrode and reference electrode were a platinum electrode and saturated calomel electrode (SCE), respectively. When the open circuit potential was stable, a dynamic polarization curve with a scan rate of 1 mV/s was obtained. Electrochemical impedance spectroscopy (EIS) was performed at a frequency range of 10^{-2}–10^5 Hz. The EIS data were fitted using ZSimDemo 3.30 software. The corrosion morphology surface was observed with SEM.

3 RESULTS

3.1 Surface morphology of the coating

Results of the three-factor and four-level orthogonal tests, considering also macroscopic morphology, coating weight and copper sulfate corrosion resistance time are shown in **Table 1**. It can be seen that the macroscopic morphology of a coating appears to be gray, ash black and black. The phosphate coating is partially non-phosphated on Samples 1 and 2. This is due to the low acid ratio and slow reaction progress. With an increase in the phosphating temperature and time, the surface of phosphate coating (Samples 3 and 4) appears gray black and smooth. Meanwhile, the surface coverage of phosphate coating is low on Samples 5 and 6. Thus, the weight of their phosphating coating is low. The phosphating reaction is slow and the phosphate coating is thin when the acid ratio is low. The acid ratio can control the equilibrium state of ionization and hydrolysis in the phosphating solution. It can be seen that Sample 8

has a gray and smooth surface, and its phosphating coating weight is 19.54 g/m^2.

As we know, the phosphating temperature is an important factor, which directly affects the speed of phosphating and the performance of phosphate coating.[19] The surface of Sample 9 is black and smooth, and its copper sulfate corrosion resistance time is 120 s. However, the surface of Sample 11 is dense, grayish black, its phosphate coating weight is 27.58 g/m^2, and its copper sulfate resistance time is 115 s. Besides, the phosphating temperature can improve the thermodynamics and dynamics of phosphate-solution molecules, which can improve the phosphating process. It can be found that the phosphate-coated surface of Sample 13 appears to exhibit an ash-like phenomenon. This may be because the acid ratio is too large, making the anodic oxidation of the metal surface too slow and the etching of the metal surface insufficient. There is a large amount of precipitation and turbidity of the phosphating solution when there is excessive hydrolysis of dihydrogen phosphate salt. Finally, the sediment floats in the phosphating solution and adheres to the 65Mn substrate to form the hanging ash phenomenon.

Table 1: Macroscopic morphology, coating weight and copper sulfate corrosion resistance time with different process parameters

No.	Acid ratio	Phosphating temperature (°C)	Phosphating time (min)	Macroscopic morphology	Evaluation	Coating weight (g/m^2)	Corrosion resistance time of copper sulfate (s)
1	4	65	3		Gray, partially non-phosphated	12.21	48
2	4	75	5		Gray, partially non-phosphated	18.44	60
3	4	85	7		Black, rich in grains	20.25	68
4	4	95	9		Light black	19.02	75
5	6	65	5		Gray, partially non-phosphated	12.5	54
6	6	75	3	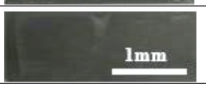	Gray, partially non-phosphated	13.87	58
7	6	85	9		Black, rich in grains	22.58	78
8	6	95	7	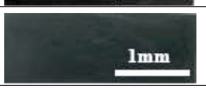	Dark gray, smooth	19.54	98
9	8	65	7	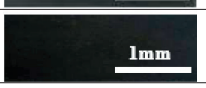	Black, smooth	21.78	120
10	8	75	9		Ash black, rough surface	24.91	90
11	8	85	3	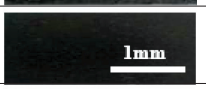	Ash black, smooth	27.58	115
12	8	95	5		Gray, partially non-phosphated	12.85	63
13	10	65	9		Off-white, hanging ash	11.54	85
14	10	75	7	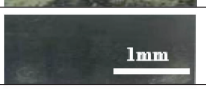	Ash black	13.05	75
15	10	85	5	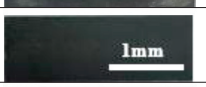	Black, smooth	22.25	132
16	10	95	3	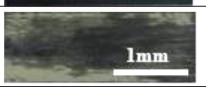	Partially non-phosphated	14.86	53

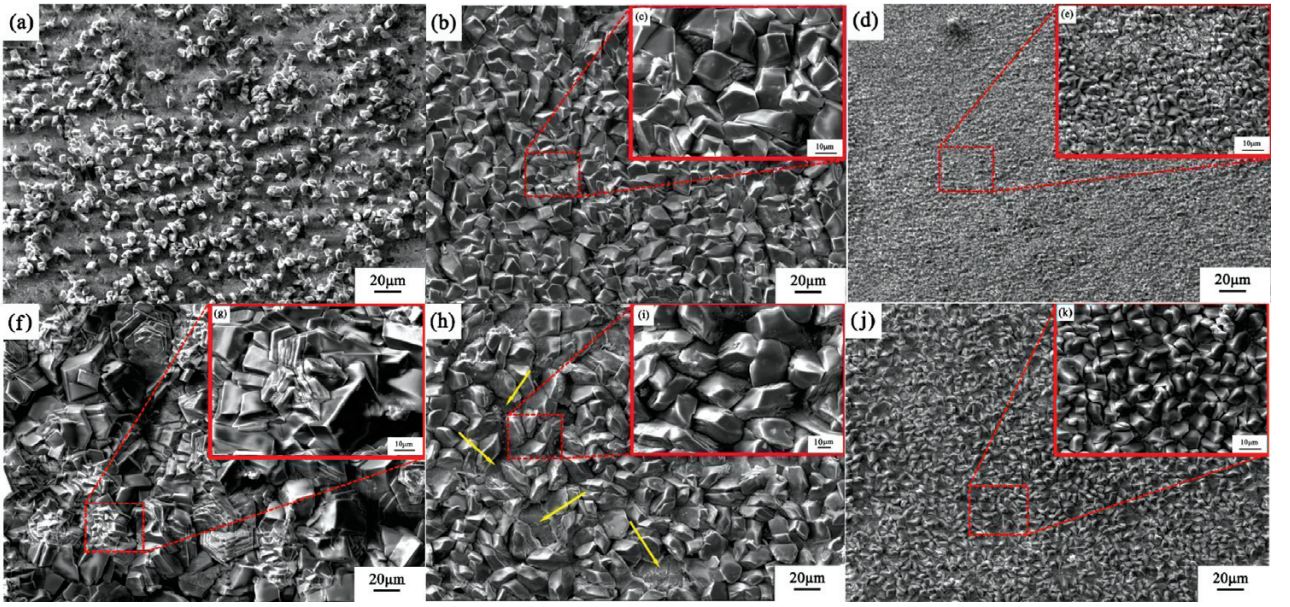

Figure 1: Scanning electron micrographs of manganese phosphate conversion coating after different phosphating processes: a) Sample 4, b) Sample 7, d) Sample 9, f) Sample 10, h) Sample 11, j) Sample 15; c), e), g), i), k) are the magnified images of the red quadrangles

In short, the microstructures and phase compositions of the phosphating surfaces were determined for Samples 4, 7, 9, 10, 11 and 15. The corrosion resistance of phosphating surfaces was examined using electrochemical corrosion and salt spray tests.

Figure 1 shows SEM morphologies of samples 4, 7, 9, 10, 11 and 15. It can be seen from **Figure 1a** that the grain gap is large and the surface coverage of phosphate coating is low when the process parameters include an acid ratio of 4, phosphating temperature of 95 °C and phosphating time of 9 min. This indicates that the phosphate coating has not been fully grown. When the phosphating temperature is reduced to 75 °C (Sample 7), the phosphate coating exhibits blocky grain crystals (of approximately 135.3 μm). It can be seen from Figure 1d that the phosphate coating surface is complete. Nevertheless, the crystal grain size is non-uniform, and some small grains cluster together. The phosphate coating has a clear, large, oblique prismatic structure when the acid ratio is 8, the phosphating temperature is 75 °C, and the phosphating time is 9 min (Sample 10). Moreover, the microstructure of Sample 11 shows a massive accumulation of crystals with a large grain size, while the coverage rate is approximately 90 %. As shown in **Figure 1h**, the non-phosphating area, indicated by the yellow arrow, is more prone to corrode. Finally, the phosphate coating grains of Sample 15 (**Figure 1j**) are fine and the grain size is about 9.98 μm. Meanwhile, Sample 15 shows a high surface coverage.

In accordance with the above analysis, **Figure 2** shows SEM morphologies and the distributions of C, Fe, Mn, O and P elements in typical phosphate coatings of Samples 7, 10 and 15. It can be seen from **Figure $2a_1$–$2f_1$** that the distribution of the C element is low and the grain size is inconsistent, while the O and Mn elements are distributed in the phosphate coating and the substrate. This indicates that the Mn and P elements infiltrated into the substrate. **Figure $2a_2$–$2f_2$** shows the dis-

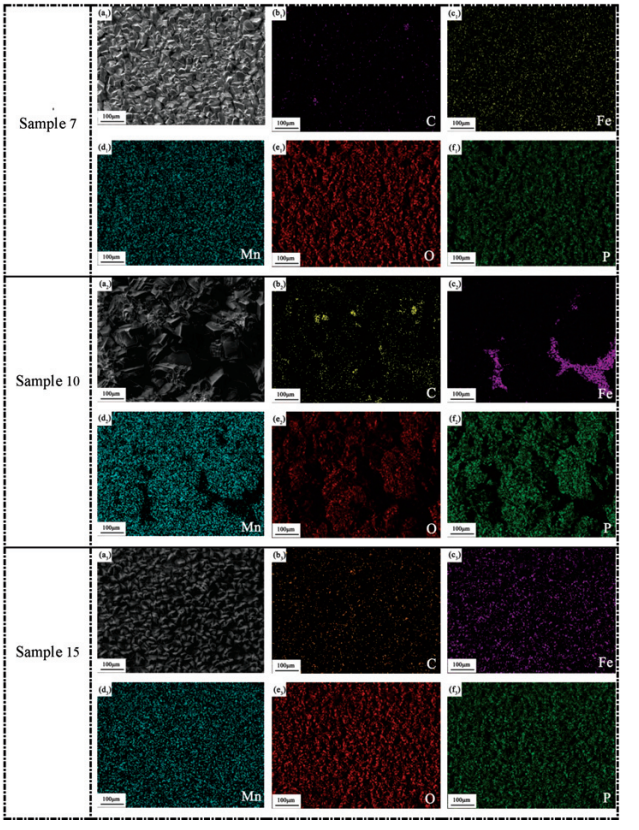

Figure 2: Surface morphology and surface element distribution of typical phosphating coating: (a_1–f_1) for Sample 7; (a_2–f_2) for Sample10; (a_3-f_3) for Sample15

tribution of elements on the phosphate coating surface of Sample 10. It can be seen that the Fe element is mainly distributed in the ravine-like grains in the bottom, indicating that the 65Mn substrate partial region has no phosphate coating. As can be seen from **Figure 2a$_3$–2f$_3$** (Sample 15), the surface grains are fine and elements C, Fe, Mn, O and P are evenly distributed. The coverage rate is higher than that of other samples. Thus, the optimal process parameters for the phosphating treatment of 65Mn spring steel are an acid ratio of 10, a phosphating temperature of 85 °C and a phosphating time of 5 min.

Figure 3 presents SEM cross-section morphologies of samples 7, 10, and 15. It can be seen that the phosphate coating is well combined with the substrate. The thickness of the phosphate coating was calculated as the average of the values obtained at three different positions using Image-pro Plus 6.0 software. The thickness of phosphate coating is about 13.82 μm (see **Figure 3a**) when the phosphating solution acid ratio is 6, phosphating temperature is 85 °C and phosphating time is 9 min. This coating thickness is due to a loose intergranular arrangement and spherical particle accumulation. As can be seen on **Figure 3b**, the phosphate coating of sample 10 has an obvious, oblique, prismatic structure and its thickness is about 9.93 μm. When the acid ratio is 10, the phosphating temperature is 85 °C and the phosphating time is 5 min, the thickness of phosphate coating (Sample 15) is 10.14 μm.

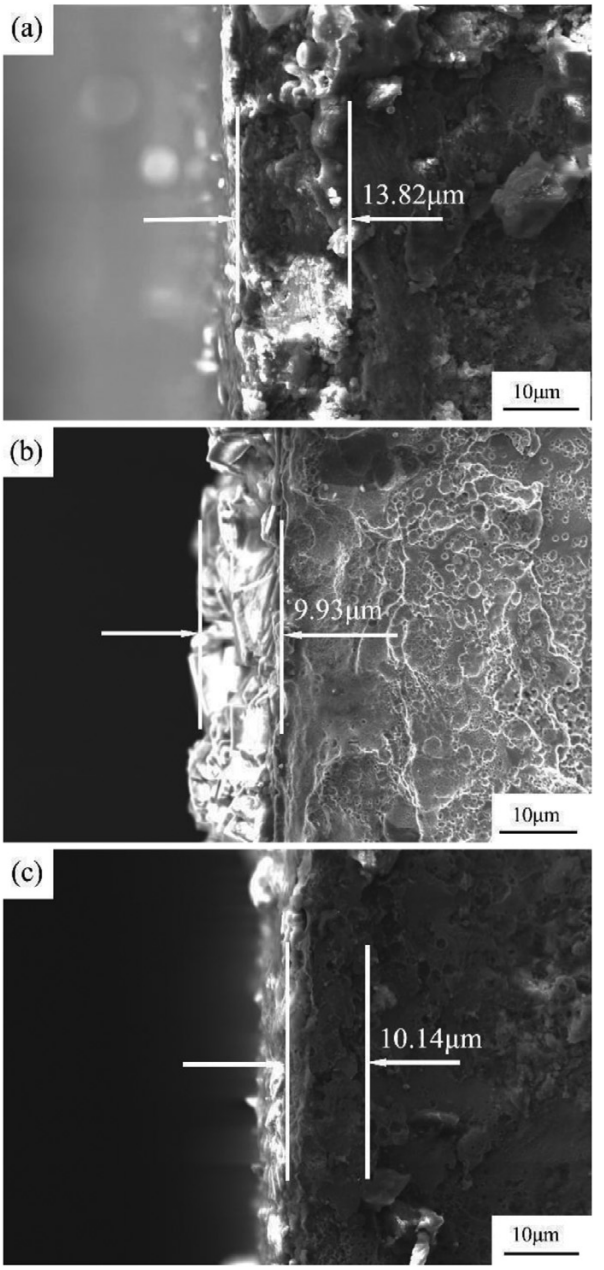

Figure 3: Cross-section morphologies of coated samples: a) Sample 7, b) Sample 10, c) Sample 15

3.2 Phase composition of the coating

Figure 4 shows the XRD patterns of 65Mn steel substrate and Samples 7, 10, and 15. Based on **Figure 4a**, the 2θ values of 44.67°, 65.02° and 82.33° are characteristic peaks of Fe corresponding to diffraction peaks of the substrate. The manganese phosphate conversion coating is composed of $Mn_5(PO_4)_2(PO_3(OH))_2{\cdot}4H_2O$ and $MnHOP_4{\cdot}2.25H_2O$ insoluble phosphate. The diffraction peaks of the $Mn_5(PO_4)_2(PO_3(OH))_2{\cdot}4H_2O$ phase can be observed at 10.11°, 26.24°, 27.61°, 30.67°, 35.34° and 36.62°, and the diffraction peaks of the $MnHOP_4{\cdot}2.25H_2O$ phase are at 10.99°, 34.06°, 35.02°, 56.02° and 58.35°. The XRD peaks of phosphate coating are basically the same, indicating that the phosphate coating has little influence on the acid ratio, phosphating temperature and phosphating time. Thus, different process parameters affect the crystallinity of the phosphate coating without changing the phase composition of the coating.

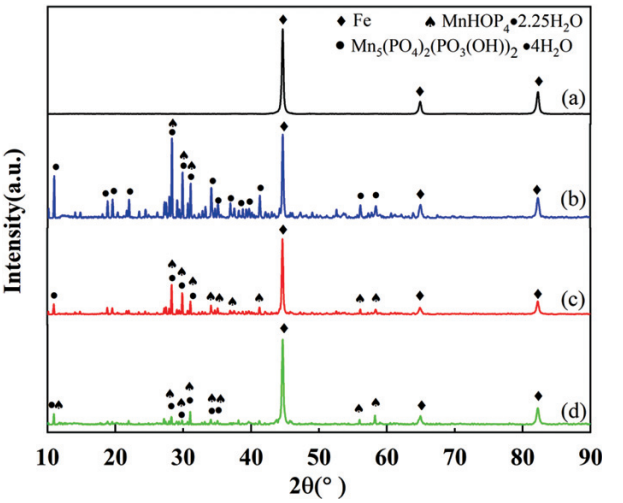

Figure 4: XRD patterns of 65Mn substrate and coated samples: a) 65Mn spring steel, b) Sample 7, c) Sample 10, d) Sample 15

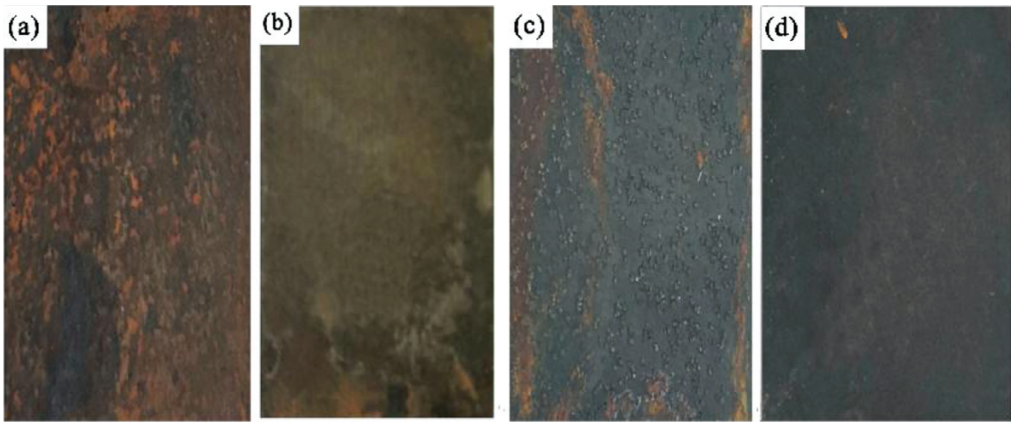

Figure 5: Surface morphologies of the samples tested using a 48-h salt spray test: a) 65Mn spring steel, b) Sample 7, c) Sample 10, d) Sample 15

3.3 Corrosion resistance performance

3.3.1 Salt spray test

Figure 5 shows the macroscopic morphologies of 65Mn substrate and Samples 7, 10 and 15 after the salt spray test for 48 h. It can be seen that there are large areas of rust on the 65Mn spring steel substrate. Nevertheless, the surface of Sample 7 includes yellow rust. Salt water is a typical electrolyte. Cl^- adsorbed on the surface of the spring steel formed a strong electric field, which accelerated the anodic dissolution of the substrate. It can also be seen on **Figure 5c** that Sample 10 has some yellow spots with a rough surface, indicating that the coating suffered local corrosion. On **Figure 5d**, it can be clearly seen that the surface of the sample is perfect, and the phosphate coating remains ash black. Phosphate coating is a non-conductive and insoluble phosphate conversion coating. It can isolate the corrosive medium from the substrate to improve the corrosion resistance of the substrate.

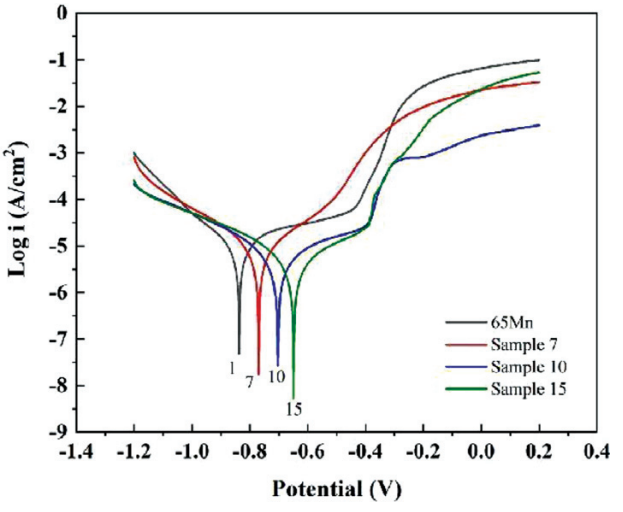

Figure 6: Tafel polarization curves of the samples measured in 3.5% NaCl solution: a) 65Mn spring steel, b) Sample 7, c) Sample 10, d) Sample15

3.3.2 Electrochemical corrosion test

Figure 6 shows the electrochemical corrosion polarization curves of 65Mn spring steel substrate, and coated samples 7, 10 and 15 in the 3.5 *w*/% NaCl solution. The anode slope (β_a), cathode slope (β_c), corrosion potential (E_{corr}) and corrosion current density (I_{corr})[20] were obtained using the Tafel curve extrapolation method, and the polarization resistance (R_p) was expressed with the Stern-Geary equation.[21,22]

$$R_p = \frac{\beta_a \beta_c}{2.303 I_{corr}(\beta_a + \beta_c)} \quad (2)$$

Electrochemical data for different specimens were calculated with the Tafel extrapolation method, as shown in **Table 2**. The electrochemical corrosion potential (E_{corr}) of the phosphate coating is higher than that of the 65Mn spring steel substrate, and the I_{corr} is 3.893×10^{-6} A/cm^2. This indicates that the corrosion resistance of the phosphate coating is better than that of the 65Mn spring steel. In addition, it can be seen from **Table 2** that the polarization resistance (R_p) of the phosphate coating is greater than that of the substrate.

Table 2: Parameters of the potentiodynamic polarization curves

	E_{coor} (V)	I_{corr} (A/cm^2)	R_p (Ω·cm^2)
65Mn steel	–0.837	1.210×10^{-5}	3744
Sample 7	–0.770	7.552×10^{-6}	5399
Sample 10	–0.703	4.443×10^{-6}	9894
Sample 15	–0.649	3.893×10^{-6}	11279

Figure 7 shows the electrochemical impedance spectroscopy (EIS) of 65Mn substrate and Samples 7, 10, 15 in the format of both Nyquist plots (**Figure 7a**) and Bode plots (**Figure 7b** and **7c**). It can be seen on **Figure 7a** that the semicircle diameters of Samples 15, 10, 7 and the 65Mn substrate are successive. Meanwhile, it is worth noting that the semicircle diameter of Sample 15 is about four times that of the 65Mn substrate. In **Figure 7b**, Sample 15 has the maximum Z value in the low-frequency region. The phase angle at a high fre-

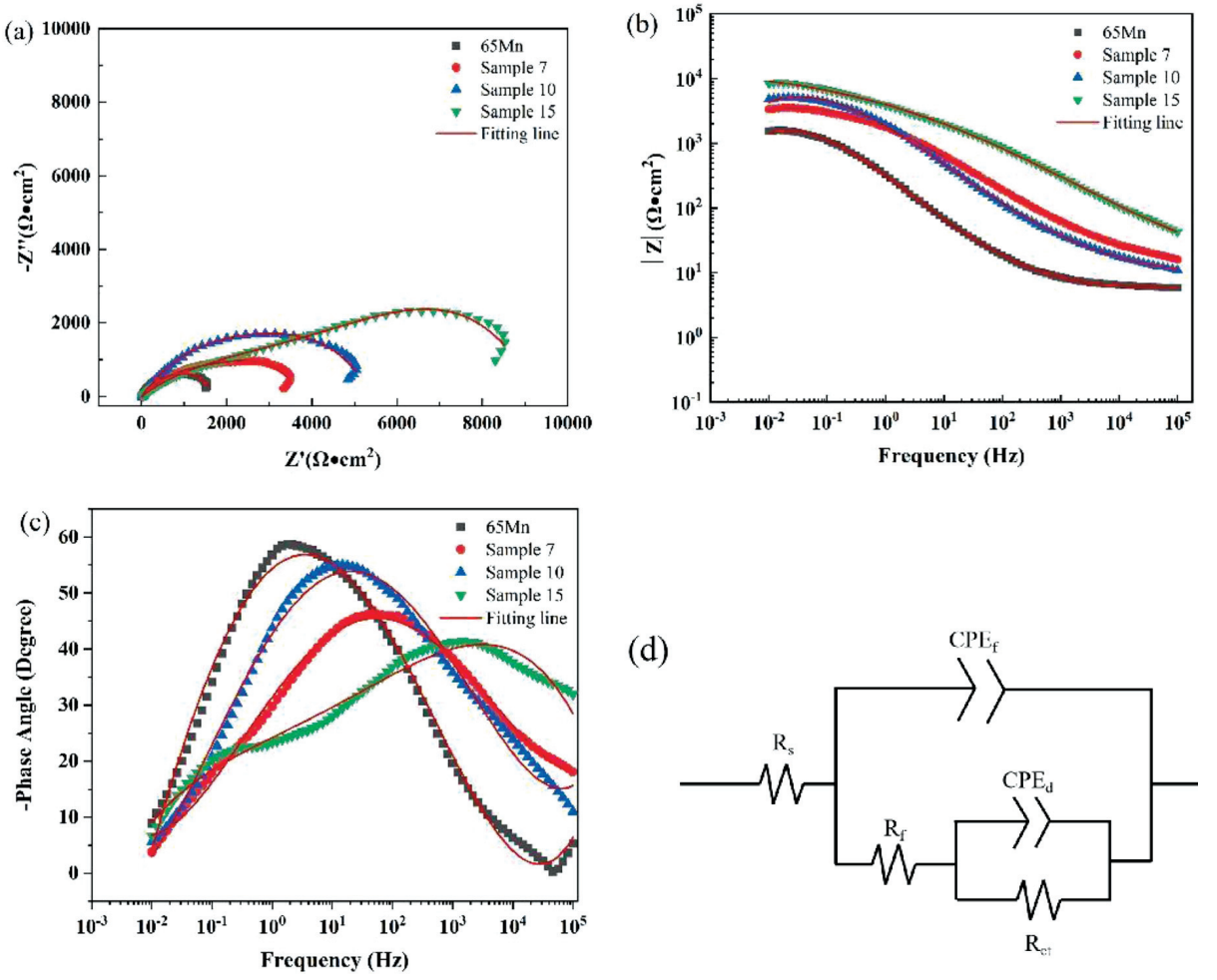

Figure 7: Electrochemical impedance: a) Nyquist plots, b) and c) Bode plots, d) equivalent circuit

quency can be used to explain the integrity of the coating.[23–24] As shown in **Figure 7c**, Sample 15 shows higher values than the 65Mn substrate in the high-frequency region, indicating that the manganese phosphating treatment can improve the corrosion resistance of the phosphate coating and reduce its defects. To obtain impedance parameters, the equivalent circuit (EC) was analyzed using ZSimDemo 3.30 software, as shown in **Figure 7d**. The fitting parameters are listed in **Table 3**. R_s values are lower than 20 Ω·cm², indicating reliable fitting data. All chi-square (χ^2) values are almost less than 0.01, indicating a high fitting degree.[25,26] Here, R_s and R_f are solution resistance and phosphate coating resistance, respectively. R_{ct} is the charge transfer resistance, while CPE_d represents a bidirectional capacitor. The slower the dissolution rate of the substrate, the greater is the R_{ct} value. In **Table 3**, the R_f value of Sample 15 is twice that of the 65Mn substrate, indicating better corrosion resistance.

Table 3: Electrochemical data obtained by equivalent circuit fitting of the EIS spectra

	65Mn	Sample 7	Sample 10	Sample 15
R_s (Ω·cm²)	6.268	9.424	9.888	16.07
CPE_f	0.0008154	0.0001171	5.715×10^{-5}	3.906×10^{-5}
n_f	0.6905	0.516	0.6645	0.5041
R_f (Ω·cm²)	1972	43.53	41.15	4138
R_{ct} (Ω·cm²)	1.182×10^{5}	3988	5558	6723
CPE_d	4.084×10^{10}	2.661×10^{-5}	6.326×10^{-5}	1.555×10^{-4}
n_d	0.7919	0.6738	0.6968	0.5688
χ^2	3.356×10^{-3}	8.774×10^{-4}	6.434×10^{-4}	7.511×10^{-4}

3.3.3 Corrosion morphology

Figure 8 shows the surface morphology of the 65Mn substrate and phosphate coating with different process parameters after immersion in the 3.5 % NaCl solution. It can be seen from **Figure 8a** that the substrate is severely corroded, having large white corrosion pits. When the phosphating solution acid ratio is 8, the phosphating temperature is 75 °C, and the phosphating time is 9 min, the substrate suffers spot corrosion when exposed to the NaCl solution. Nevertheless, it can be seen that Sample 15 maintains fine gray-black grains with some NaCl particles. Phosphate conversion coating is insoluble and non-conductive, and can prevent the corrosion of 65Mn spring steel.

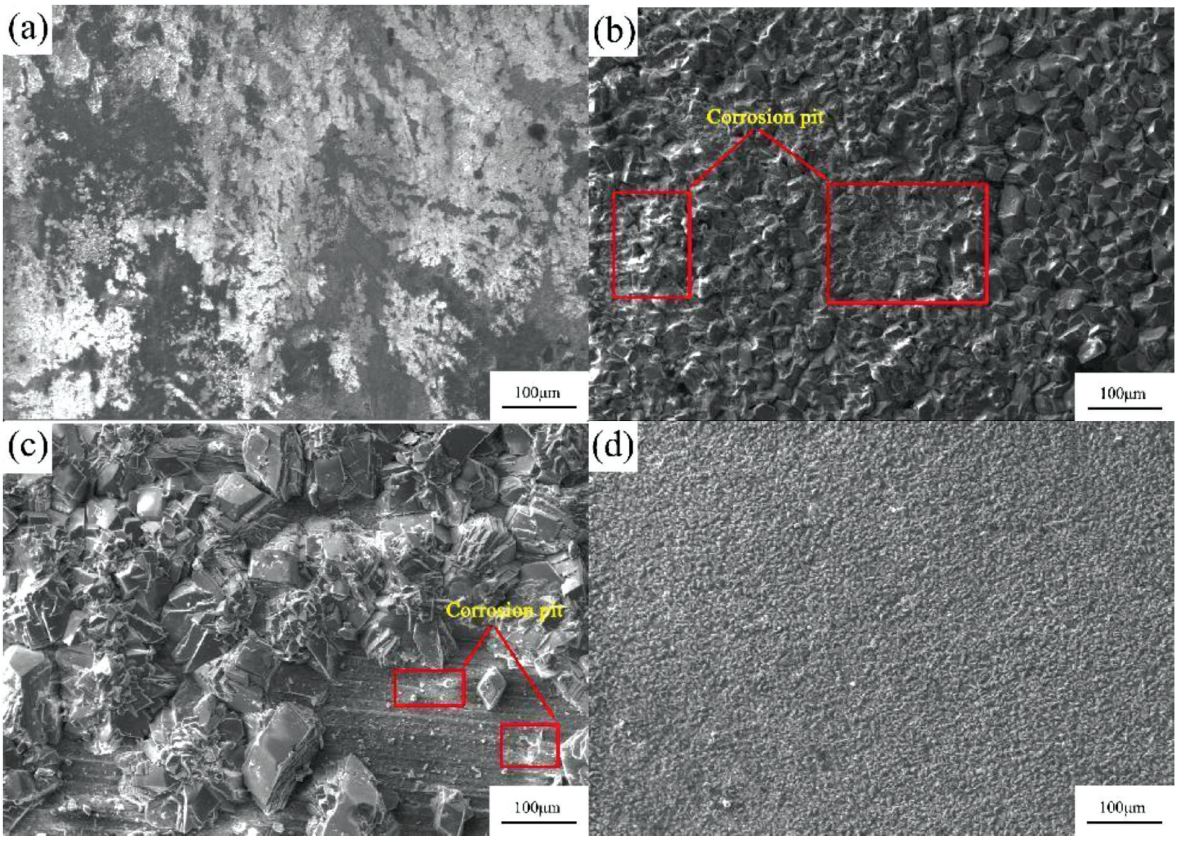

Figure 8: Corrosion morphologies of the samples after immersion in 3.5 *w*/% NaCl solution: a) 65Mn spring steel, b) Sample 7, c) Sample 10, d) Sample 15

4 DISCUSSION

4.1 Formation mechanism of the manganese phosphate coating

In the present study, the manganese phosphate coating was prepared on the 65Mn spring steel. Phosphating is a complex chemical reaction process, which is also an electrochemical reaction. To further understand the phosphate coating forming process, the formation mechanism can be illustrated with the schematic diagram shown in **Figure 9**. The formation of the manganese phosphate coating consists of two parts.[27] The first step is the micro-battery reaction (**Figure 9a**), which includes the dissolution of the 65Mn spring steel anode and the reaction of cathode hydrogen evolution. When the 65Mn spring steel is immersed in a phosphating solution, Fe begins to dissolve and H^+ releases hydrogen gas. The chemical reactions are as follows:

anode reaction: $Fe \rightarrow Fe^{2+} + 2e^-$ (3)

cathode reaction: $2H_2O + 2e^- \rightarrow 2OH^- + H_2$ (4)

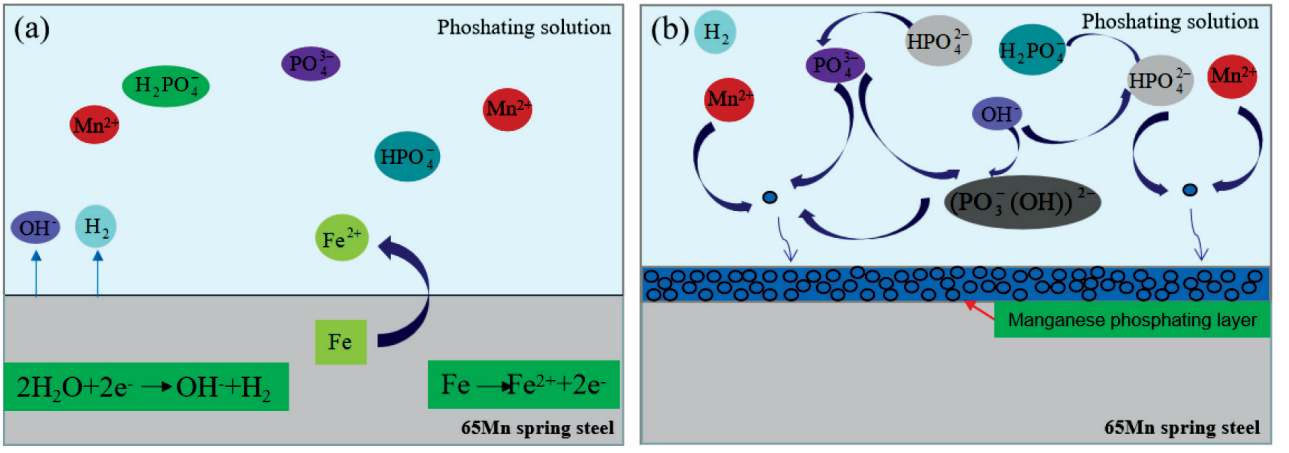

Figure 9: Diagram of phosphate coating on the 65Mn spring steel surface

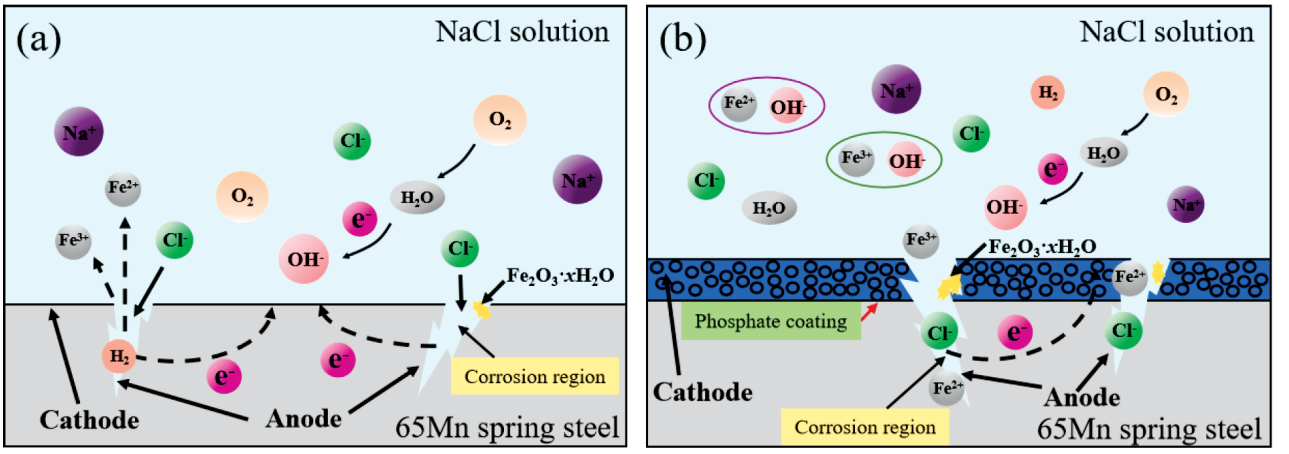

Figure 10: Diagram of the corrosion of 65Mn spring steel and manganese phosphate coating

overall reaction: $Fe + 2H_2O \rightarrow Fe^{2+} + H_2 + 2OH^-$ (5)

The phosphoric acid solution dissociates into PO_4^{3-}, $H_2PO_4^{3-}$, HPO_4^{2-}, and other ions. Therefore, there is an increase in the pH value of the solution. Fe^{2+}, PO_4^{3-}, OH^-, HPO_4^{2-} and Mn^{2+} can react and form an insoluble phosphate. Mn^{2+} and HPO_4^{2-} are involved in the reaction to form $MnHOP_4{\cdot}2.25H_2O$ crystals. Mn^{2+}, PO_4^{3-} and HPO_4^{2-} react to form $Mn_5(PO_4)_2(PO_3(OH))_2{\cdot}4H_2O$ (see **Figure 4**). The responses are as follows:

$$Mn^{2+} + HPO_4^{2-} + 2.25H_2O \rightarrow MnHPO_4 \cdot 2.25H_2O \quad (6)$$

$$5Mn^{2+} + 2PO_4^{3-} + 2(PO_3(OH))^{2-} + 4H_2O \rightarrow \rightarrow Mn_5(PO_4)_2(PO_3(OH))_2 \cdot 4H_2O \quad (7)$$

There is an insoluble phosphate and a dense coating structure composed of $Mn_5(PO_4)_2(PO_3(OH))_2 \cdot 4H_2O$ and $MnHOP_4 \cdot 2.25H_2O$.[28–30] As mentioned above, the density of the coating is the key factor affecting the acid ratio and phosphating temperature.

4.2 Corrosion behavior of the manganese phosphate coating

Figure 10 shows the diagram of the corrosion of 65Mn spring steel and manganese phosphate coating immersed in the 3.5 % NaCl solution. This is the Pourbaix diagram of the Fe - H_2O system.[31] The cathodic reaction of the sample is mainly an oxygen reduction reaction and the anode solution of Fe into Fe^{2+}. The reaction equation is given below:

$$O_2 + 2H_2O + 4e^- \rightarrow 4OH^- \quad (9)$$

$$Fe \rightarrow Fe^{2+} + 2e^- \quad (10)$$

During the anode reaction, Fe^{2+} combines with OH^- to from $Fe(OH)_3$, which then continues to hydrolyze into $Fe(OH)_3$ and becomes $Fe_2O_3 \cdot xH_2O$ rust. The relevant equations are expressed as follows:

$$Fe^{2+} + 2OH^- \rightarrow Fe(OH)_2 \quad (11)$$

$$4Fe(OH)_2 + 2H_2O \rightarrow 4Fe(OH)_3 \quad (12)$$

$$2Fe(OH)_3 \rightarrow Fe_2O_3 \cdot xH_2O + (3 - x)H_2O \quad (13)$$

When 65Mn spring steel is directly immersed in the NaCl solution, E_{corr} exceeds the corrosive pitting of the material, and corrosive pitting begins to occur on the ferrite. Cl^- corrosive anions continuously enter the corrosion pits, causing the pitting growth to expand.[32–34] Eventually, large areas of corrosion are formed (**Figure 8a**). **Figure 10b** shows the diagram of the corrosion process of manganese phosphating coating. The corrosion is due to the low coverage of 65Mn spring steel exposed to the NaCl solution (see **Figures 1f-1h** and **2a$_2$-2f$_2$**). Cl^- ions erode 65Mn steel, resulting in the substrate being corroded. According to the above, manganese phosphate coating can guarantee good corrosion resistance when it has high coverage and a fine grain size. Meanwhile, it is classified as an insoluble phosphate.[35,36] Thus, the phosphate coating on the surface of Sample 15 has a fine grain size, enhancing the anti-corrosion of the substrate.

5 CONCLUSIONS

Manganese phosphate conversion coatings were prepared on 65Mn spring steel. The surface morphology, microstructure, and corrosion behavior of the coating were investigated. The main conclusions are as follows:

The macroscopic morphology of the coating presents gray, ash black and black colors. With an increase in the phosphating temperature and time, the surface of phosphate coating becomes gray black and smooth.

The microstructure shows blocky grain crystals, massive grain accumulation crystals, and an oblique prismatic structure, all resulting from different phosphating process parameters. Elements C, Fe, Mn, O and P are evenly distributed, and the surface grain size is well distributed.

The XRD pattern shows that manganese phosphating coating is mainly composed of the $Mn_5(PO_4)_2(PO_3(OH))_2{\cdot}4H_2O$ and $MnHOP_4{\cdot}2.25H_2O$ phase. Furthermore, the phase composition of the coating is not affected by the phosphating process parameters.

There was a large area of yellow rust on the 65Mn steel substrate after salt spray for 48 h. However, there were no obvious signs of corrosion on the phosphating-coated surface when the acid ratio was 10, the phosphating temperature was 85 °C, and the phosphating time was 5 min. Meanwhile, the coating maintained fine gray-black grains.

Acknowledgment

This work is supported by the Qin Chuang Yuan Innovation Talent Program of Shaanxi (QCYRCXM-2023-036, QCYRCXM-2023-032 and QCYRCXM-2022-290), Natural Science Basic Research Program of Shaanxi (2024JC-YBQN-0461 and 2024JC-YBQN-0114), and Key Research and Development Program of Shaanxi (No. 2024GX-YBXM-343).

6 REFERENCES

[1] Y. J. Wang, J. J. Sun, T. Jiang, C. Yang, Q. Tan, S. W. Guo, Y. N. Liu, Super strength of 65Mn spring steel obtained by appropriate quenching and tempering in an ultrafine grain condition, Mater. Sci. Eng. A, 754 (**2019**) 1–8, doi:10.1016/j.msea.2019.03.059

[2] P. F. Zhang, D. C. Wang, P. Cheng, C. X. Shao, J. Y. Zhou, J. H. Huang, Warm-deformation behavior of 65Mn spring steel, Mater. Tehnol., 55 (**2021**) 5, 717–724, doi:10.17222/mit.2021.193

[3] P. F. Zhang, D. C. Wang, Y. Guo, P. Cheng, C. X. Shao, N. Lang, X. X. Liu, Fatigue failure analysis and finite element assessment of the twins torsion spring, Eng. Fail. Anal., 122 (**2021**), 105187, doi:10.1016/j.engfailanal.2020.105187

[4] Z. Yao, Z. Z. Huang, S. Lyu, F. Q. Tang, B. J. Zhao, X. D. Ma, Characterization and strengthening mechanism of high-strength medium carbon spring steels, J. Mater. Res. Technol., 27 (**2023**), 1395–1405, doi:10.1016/j.jmrt.2023.09.314

[5] V. C. Gudla, R. Ambat, Corrosion failure analysis of hearing aid battery-spring contacts, Eng. Fail. Anal., 79 (**2017**), 980–987, doi:10.1016/j.engfailanal.2017.05.045

[6] X. H. Lv, Y. D. Yang, D. C. Zhang, Z. L. Wang, K. L. Li, W. F. Rao, A ratchet spring structure can harvest waves with variable frequencies, Mater. Today Comm., 30 (**2022**), 103175, doi:10.1016/j.mtcomm.2023.105386

[7] S. Barella, A. Gruttadauria, C. Mapelli, Anomalous corrosion phenomena observed on electrovalves of coffee espresso machines, Eng. Failure Anal., 5 (**2013**), 449–456, doi:10.1016/j.engfailanal.2013.06.025

[8] V. Singh, A. Zolfaghari, M. Marya, A comparative parametric investigation of thin diamond-like and polymer-like carbon coatings to explore carbonate anti-scaling performance, Surf. Coat. Tech., 473 (**2023**), 130015, doi:10.1016/j.surfcoat.2023.130015

[9] Y. Guo, J. H. Zhao, J. X. Zhang, C. Gu, Y. J. Wang, Fe-Mn-xCr-Al-Si steel with multi-layer magnetic structure fabricated by oxidation treatment, Mater. Today Comm., 34 (**2023**), 105283, doi:10.1016/j.mtcomm.2022.105283

[10] W. Z. Wang, S. S. Feng, Z. M. Li, Z. G. Chen, T. Y. Zhao, Microstructure and properties of micro-arc oxidation ceramic films on AerMet100 steel, J. Mater. Res. Tech., 3 (**2022**), 6014–6027, doi:10.1016/j.jmrt.2020.04.005

[11] T. M. Gong, P. P. Yao, X. T. Zuo, Z. Y. Zhang, Y. L. Xiao, L. Zhao, H. B. Zhou, M. W. Deng, Q. Wang, A. W. Zhong, Influence of WC carbide particle size on the microstructure and abrasive wear behavior of WC-10Co-4Cr coatings for aircraft landing gear, Wear, 362 (**2016**), 135–145, doi:10.1016/j.wear.2016.05.022

[12] X. J. Cui, C. H. Liu, R. S. Yang, Q. S. Fu, X. Z. Lin, M. Gong, Duplex-layered manganese phosphate conversion coating on AZ31 Mg alloy and its initial formation mechanism, Corros. Sci., 76 (**2013**), 474–485, doi:10.1016/j.corsci.2013.07.024

[13] R. C. Zeng, Z. D. Lan, L. H. Kong, Y. D. Huang, H. Z. Cui, Characterization of calcium-modified zinc phosphate conversion coatings and their influences on corrosion resistance of AZ31 alloy, Surf. Coat. Technol., 205 (**2011**), 3347–3355, doi:10.1016/j.surfcoat.2010.11.027

[14] S. Shanmugam, K. Ravichandran, T. S. N. Sankara Narayanan, M. Marappan, Development of permanganate assisted manganese phosphate coating on mild steel, Corros. Eng. Sci. Techn., 49 (**2014**), 719–726, doi:10.1179/1743278214Y.0000000169

[15] L. H. Guo, Q. Huang, C. Zhang, J. Wang, G. P. Shen, C. L. Ban, L. X. Guo, Study on the formation of Mn-P coatings with significant corrosion resistance on Q235 carbon steels by adjusting the ratio of phosphorus to manganese, Corros. Sci., 178 (**2021**), 108960, doi:10.1016/j.corsci.2020.108960

[16] H. Nikdehghan, A. Amadeh, A. Honarbakhsh-Raouf, Effect of substrate heat treatment on morphology and corrosion resistance of Zn-Mn phosphate coating, Surf. Eng., 24 (**2013**), 287–294, doi:10.1179/174329408X326533

[17] H. Y. Su, C. S. Lin, Effect of additives on the properties of phosphate conversion coating on electrogalvanized steel sheet, Corros. Sci., 83 (**2014**), 137–146, doi:10.1016/j.corsci.2014.02.002

[18] L. B. Zang, Y. Chen, Y. M. Wu, Y. Zheng, H. Chen, D. L. You, L. Li, J. K. Li, Comparative tribological and friction behaviors of oil-lubricated manganese phosphate conversion coatings with different crystal sizes on AISI 52100 steel, Wear, 458–459 (**2020**), 203427, doi:10.1016/j.wear.2020.203427

[19] K. B. Xu, B. Y. Wu, J. L. Wan. A potentiometric phosphate ion sensor based on electrochemically modified nickel electrode, Electrochim. Acta, 412 (**2022**), 140065, doi:10.1016/j.electacta.2022.140065

[20] Y. X. Li, P. F. Zhang, P. K. Bai, Microstructure and properties of Ti/TiBCN coating on 7075 aluminum alloy by laser cladding, Surf. Coat. Tech., 334 (**2018**), 142–149, doi:10.1016/j.surfcoat.2017.11.034

[21] Y. Guo, Y. Q. Zhang, Z. Y. Li, Microstructure and properties of in-situ synthesized ZrC-Al3Zr reinforced composite coating on AZ91D magnesium alloy by laser cladding, Surf. Coat. Tech., 334 (**2018**), 471–478, doi:10.1016/j.surfcoat.2017.12.007

[22] L. F. Xie, W. L. Zhou, S. W. Zou, Pitting behavior of Ti-15-3 titanium alloy with different surface in salt spray studied using electrochemical noise, J. Mater. Res. Technol., 14 (**2021**), 2865–2883, doi:10.1016/j.jmrt.2021.08.072

[23] G. L. Liu, C. Z. Huang, B. Zou, The modification of corrosion resistance of 17-4PH stainless steel by cutting process, J. Manuf. Process., 49 (**2020**), 447–455, doi:10.1016/j.jmapro.2019.11.001

[24] R. Amini, A. A. Sarabi, The corrosion properties of phosphate coating on AZ31 magnesium alloy: the effect of sodium dodecyl sulfate (SDS) as an eco-friendly accelerating agent, App. Surf. Sci., 257 (**2011**), 7134–7139, doi:10.1016/j.apsusc.2011.03.072

[25] C. Y. Tsai, J. S. Liu, P. L. Chen, Chao-Sung Lin, Effect of Mg^{2+} on the microstructure and corrosion resistance of the phosphate conversion coating on hot-dip galvanized sheet steel, Corros. Sci., 52 (**2010**), 3907–3916, doi:10.1016/j.corsci.2010.08.007

[26] L. Y. Li, L. Y. Cui, B. Liu, et al., Corrosion resistance of glucose-induced hydrothermal calcium phosphate coating on pure magnesium, Appl. Surf. Sci., 465 (**2019**), 1066–1077, doi:10.1016/j.apsusc.2018.09.203

[27] H. Yin, F. Liu, X. H. Chen, Synthesis of hureaulite by a reflux process at ambient temperature and pressure, Micropor. Mesopor. Mat., 153 (**2012**), 115–123, doi:10.1016/j.micromeso.2011.11.057

[28] P. Hivart, B. Hauw, J. P. Bricout, et al., Seizure behaviour of manganese phosphate coatings according to the process conditions, Tribol. Int., 30 (**1997**) 8, 561–570, doi:10.1016/S0301-679X(97)00019-4

[29] H. I. Hsiang, L. T. Mei, Y. H. Lin, Formation and growth of manganese phosphate passivation layers for NTC ceramics, J. Alloys Compd., 484 (**2009**), 723–728, doi:10.1016/j.jallcom.2009.05.026

[30] C. M. Wang, W. T. Tsai, Y. P. Lee, Morphological and microstructural evolutions of manganese phosphate coating formed in Ni^{2+} ion containing electrolyte, Surf. Eng., 24 (**2008**), 392–397, doi:10.1179/026708408X323034

[31] D. X. Wen, P. Long, J. J. Li, Effects of linear heat input on microstructure and corrosion behavior of an austenitic stainless steel processed by wire arc additive manufacturing, Vacuum, 173 (**2020**), 109131, doi:10.1016/j.vacuum.2019.109131

[32] P. Cheng, Y. H. Zhao, R. P. Lu, H. Hou, Effect of the morphology of long-period stacking ordered phase on mechanical properties and corrosion behavior of cast Mg-Zn-Y-Ti alloy, J. Alloys Compd., 764 (**2018**), 226–238, doi:10.1016/j.jallcom.2018.06.056

[33] L. F. Xie, W. L. Zhou, B. Zhou, S. Bi, P. F. Zhang, Q. W. Tian, Z. D. Yu, Exploring salt-mist corrosion resistance of GPTMS functionalized graphene oxide reinforced epoxy resin composite coating on shot-peened Ti-15333 titanium alloy, Surfaces and Interfaces, 44 (**2024**), 103675, doi:10.1016/j.surfin.2023.103675

[34] M. Fouladi, A. Amadeh, Effect of phosphating time and temperature on microstructure and corrosion behavior of magnesium phosphate coating, Electrochim. Acta, 106 (**2013**), 1–12, doi:10.1016/j.electacta.2013.05.041

[35] G. X. Wang, N. N. Cao, Y. Y. Wang, Characteristics and corrosion studies of zinc–manganese phosphate coatings on magnesium–lithium alloy, RSC Adv., 4 (**2014**), 59772–59778, doi:10.1039/C4RA08122F

[36] M. Mahdavian, M. M. Attar, Another approach in analysis of paint coatings with EIS measurement: phase angle at high frequencies, Corros. Sci., 48 (**2006**), 4152–4157, doi:10.1016/j.corsci.2006.03.012